CrossMark

High-temperature deformation behavior of a beta Ti–3.0Al–3.5Cr–2.0Fe–0.1B alloy

Wen-Tao Qu, Xu-Guang Sun, Song-Xiao Hui, Zhen-Guo Wang, Yan Li*

Abstract The high-temperature deformation behavior of a beta Ti–3.0Al–3.5Cr–2.0Fe–0.1B alloy was investigated by a Gleeble-1500D thermal simulator. The height reduction was 50%, corresponding to a true strain of 0.693. The strain rate ranging from 0.01 to 10.00 s^{-1} and the deformation temperature ranging from 800 to 950 °C were considered. The flow stress and the apparent activation energy for deformation, along with the constitutive equation, were used to analyze the behavior of the Ti–3.0Al–3.5Cr–2.0Fe–0.1B alloy. The processing map was established. The effect of strain rate on the microstructure at 850 °C was evaluated. The flow stress–strain curves indicated that the peak flow stresses increased along with an increase in the strain rate and decreased as the deformation temperature increased. Based on the true stress–true strain curves, the constitutive equation was established and followed as the $\dot{\varepsilon} = 6.58 \times 10^{10}[\sinh(0.0113\sigma)]^{3.44}\exp(-245481.3/RT)$. The processing map exhibited the "unsafe" region at the strain rate of 10 s^{-1} and the temperature of 850 °C, and the rest region was "safe". The deformation microstructure demonstrated that both dynamic recovery (DRV) and dynamic recrystallization (DRX) existed during deformation. At the lower strain rate of 0.01 s^{-1}, the main deformation mechanism was the DRV, and the DRX was the dominant deformation mechanism at the higher strain rate of 1.00 s^{-1}.

Keywords Titanium alloy; Hot deformation; Constitutive equation; Processing map; Microstructure

1 Introduction

The titanium alloys have been widely utilized in aerospace, automotive, chemical and military industries, due to the corresponding favorable material properties such as low density, high specific strength, excellent fracture toughness and corrosion resistance [1–3]. As it is well known, the microstructural evolution and properties of titanium alloys are sensitive to process parameters, such as deformation temperature and strain rate, which have significant effects on the forming characteristics and the target products quality [3–11]. The behavior and microstructure of titanium alloys during hot compressive deformation are complex and change along with the process parameters [6, 7]. Sun et al. [4] pointed out that the microstructure and dynamic properties of the TA15 alloys are quite sensitive to the process parameters, which directly determine the service properties. Lei et al. [5] demonstrated that the deformation temperature plays an important role in the stress-induced martensite transformation in TB6 alloys. Hua et al. [7] researched the microstructural characterization of Ti-5553 alloys, demonstrating that the deformation parameters could significantly affect the microstructural evolution, whereas the dynamic recrystallization was quite noticeable at the temperature of 900 °C and the strain rate of 1×10^{-3} s^{-1}. The Ti–5Al–5Mo–5V–2Nb–1Fe–1Zr [8],

W.-T. Qu, X.-G. Sun
School of Mechanical Engineering, Xi'an Shiyou University,
Xi'an 710065, China

S.-X. Hui
State Key Laboratory of Nonferrous Metals and Processes,
General Research Institute for Nonferrous Metals, Beijing
100088, China

Z.-G. Wang, Y. Li*
School of Materials Science and Engineering, Beihang
University, Beijing 100191, China
e-mail: liyan@buaa.edu.cn

⚡ Springer

Ti–6Al–4V [9] and Ti–6Al–2Sn–2Zr–3Mo–1Cr–2Nb–Si [11] alloys also are sensitive to both deformation temperature and strain rate.

The Ti–Al–Cr–Fe–(B) is a newly developed titanium alloy [2, 6, 12–14], where the microstructure and tensile properties were studied, demonstrating high ultimate strength and good elongation [2, 12, 13]. The hot compressive behaviors of Ti–Al–Cr–Fe–(B) alloys were investigated by isothermal compression from 800 to 950 °C at the strain rates of 0.01–10.00 s^{-1} [6, 14]. In contrast, in practical applications, the titanium alloys are processed into the target products, requiring different or multiple deformations. Hence, experiments and investigations are still required for an improved comprehension of the hot deformation behavior of these alloys. In this study, the isothermal compression behavior of the Ti–3.0Al–3.5Cr–2.0Fe–0.1B alloys at the true strain of 0.693 (compress 50%) was researched. The effects of deformation temperature and strain rate on the flow stress were investigated. The apparent activation energy for deformation was calculated. The constitutive equation was developed, and the processing map along with the microstructural observation was established. Also, the microstructural evolution at 850 °C under various strain rates was observed.

2 Experimental

The target alloy was Ti–3.0Al–3.5Cr–2.0Fe–0.1B with the chemical composition of 2.96 wt% Al, 3.48 wt% Cr, 2.04 wt% Fe, 0.10 wt% B and the balance element was Ti. The β phase transformation temperature was (885 ± 5) °C. The optical microscope (OM) image of the initial Ti–3.0Al–3.5Cr–2.0Fe–0.1B alloy microstructure with equiaxed β and a little α phase is presented in Fig. 1.
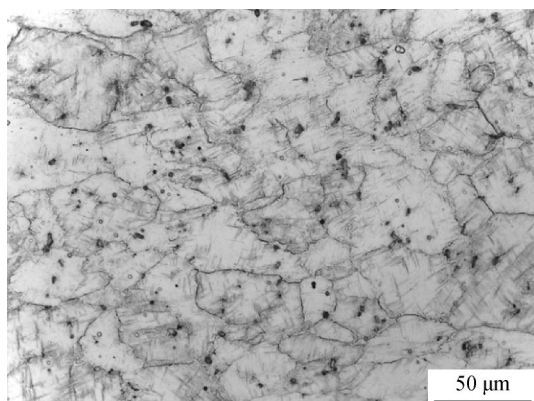

Fig. 1 OM image of initial Ti–3.0Al–3.5Cr–2.0Fe–0.1B alloy

Cylindrical compression samples with 8 mm in diameter and 12 mm in height were prepared, as presented in Fig. 2a. The isothermal single-hit hot compression experiments were performed on the Gleeble-1500D thermal simulator (Tsinghua University, China). Four deformation temperatures (800, 850, 900 and 950 °C) and four strain rates (0.01, 0.10, 1.00 and 10.00 s^{-1}) were employed. The samples were compressed to 50% of the initial height, corresponding to the true strain of 0.693, as presented in Fig. 2b. And the alloy has been studied under the compress of 70% in Ref. [6], while the rest experimental conditions are the same as those in this reference. Thermocouples were welded on the sample surfaces for the actual temperature measurement during testing. The sample ends were covered by an appropriate lubricant consisting of graphite pieces to reduce the friction effects between each sample and the flat. Prior to testing, the samples were reheated to the testing temperature of 5 °C·s^{-1} and retained for 5 min to obtain a uniform temperature. The stress–strain data were automatically recorded by the test system. Consequently, the samples were water-quenched to preserve the deformed microstructure. Then, the samples were severed parallel to the compression axis for the microstructural analysis. Subsequently to polishing and etching in a Kroll's reagent (volume ratio of HF:HNO$_3$:H$_2$O = 1:3:7), the microstructures were examined by a Zeiss OM (Axiovert 200 MAT).

3 Results and discussion

3.1 True stress–true strain curves

Figure 3 presents the typical true flow stress–strain curves during the isothermal compression of the Ti–3.0Al–3.5Cr–2.0Fe–0.1B alloys. The corresponding peak flow stress values are listed in Table 1. It could be observed that the alloy is sensitive to the strain rate and the deformation temperature. The peak flow stresses increase as the strain rate increases and decrease as the deformation temperature
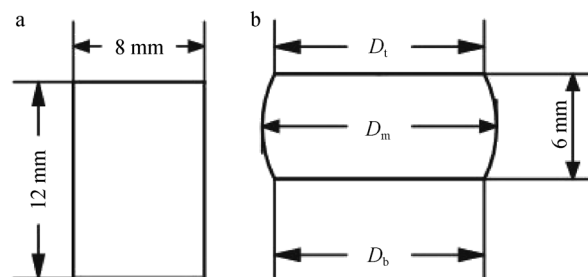

Fig. 2 Dimensions measured in sample **a** before and **b** after deformation (D_t, diameter for drum top; D_m, diameter for drum belly; D_b, diameter for drum bottom)
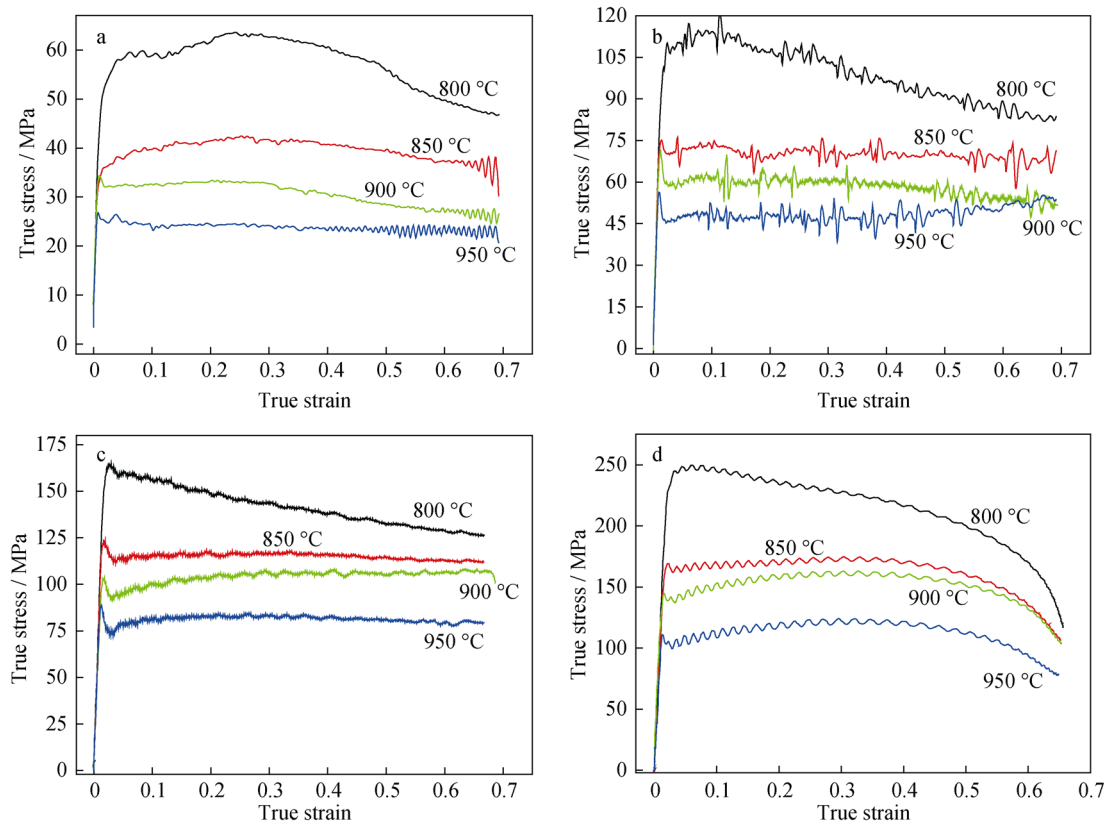
Fig. 3 Typical true stress–strain curves obtained at different strain rates and deformation temperatures: **a** 0.01 s^{-1}, **b** 0.10 s^{-1}, **c** 1.00 s^{-1}, and **d** 10.00 s^{-1}

Table 1 Peak flow stress of Ti–3.0Al–3.5Cr–2.0Fe–0.1B alloy under different conditions

Strain rate/s^{-1}	Peak flow stress/MPa			
	800 °C	850 °C	900 °C	950 °C
0.01	63.56	42.43	34.32	26.79
0.10	106.42	76.10	71.03	56.34
1.00	159.76	123.54	108.27	88.61
10.00	249.67	174.75	163.08	124.16

increases. At the beginning of the flow stress–strain curves, the flow stress rapidly reaches the peak stress due to work hardening (WH) [9, 15]. Simultaneously, the dynamic recovery (DRV) was utilized to minimize the WH. A competition between WH and DRV softening is apparent. At the lower deformation temperature, WH plays a more significantly important role than DR in the stress, whereas the stress increases significantly along with the strain. As the temperature increases, DRV effects increase [9]. The flow stress–strain curves reach a fairly constant level as the strain increases, as presented in Fig. 3, due to the competition between WH and softening mechanisms, reaching a relative balance [15]. This phenomenon results in the flow stress–strain curves, displaying the sawtooth characteristic

at the higher strain rate of 10.00 s^{-1} (Fig. 3d). In the material structure, a high amount of dislocations is generated under the applied stress; the obstacles of dislocation blocks, jogs and tangles which were produced by the dislocation motion could inhibit the dislocation motion, whereas subsequently the WH occurs, increasing the material deformation resistance [16, 17].

Owing to the titanium alloy lower thermal conductivity, the heat which is induced by plastic deformation could not be diffused quickly and results in a temperature increase [18]. As the strain and temperature increase, the softening effect causes the flow stress to decrease and tend toward a steady state. Owing to the increased atom thermal motion, a higher energy fluctuation increases the dislocation motion and the DRV or dynamic recrystallization (DRX) occurrence, where a portion of the WH effect is counterbalanced, resulting in a flow stress decrease.

As presented in Fig. 1, the β phase with a slight α phase is included in Ti–3.0Al–3.5Cr–2.0Fe–0.1B alloy microstructure. As it is well known, the deformation of hcp-α phase is harder to occur compared to that of bcc-β phase. During deformation, the α phase acts as a hard phase and might have resulted in a pinning effect for the dislocations [19]. It could be one of the reasons which induce

the increase in rapid flow stress [20]. As the deformation continues, the flow stress increases, the dislocations produce slips, leading to a flow stress decrease [21].

At a certain strain rate, as presented in Table 1, the peak flow stress decreases as the deformation temperature increases. This is mainly due to the enhanced thermal activation of the alloy, and the average kinetic energy per atom increases as the deformation temperature increases. Also, a higher amount of critical slips occur, whereas the cross-slip and the grain boundary migration ability increase. Furthermore, it is well known that the bcc-β phase in titanium alloys has higher stacking fault energy, where the dislocation climb and the cross slips occur quite easily, which could be counteracted the WH caused by the dislocation multiplication [6, 22]. At a given deformation temperature, as presented in Table 1, the peak flow stress increases as the strain rate increases. The main reason is that the dislocation multiplication rate increases significantly, as the strain rate increases. Moreover, the tangled dislocation structures inhibit the dislocation movement, resulting in an increase in flow stress during the Ti–3.0Al–3.5Cr–2.0Fe–0.1B alloy isothermal compression [11].

As compared with the peak flow stress values in Ref. [6], which were obtained under the deformation of 70%, there is no regular change with the change of deformation. The results show that the deformation also influences the flow stress of the alloy.

3.2 Constitutive equation

The constitutive equations, related to flow stress, strain rate, strain and temperature, were developed for the hot compression behavior of the alloys to be understood [6, 23].

$$\dot{\varepsilon} = A[\sinh \alpha\sigma]^n \exp\left(-\frac{Q}{RT}\right) \tag{1}$$

$$Z = A[\sinh \alpha\sigma]^n = \dot{\varepsilon} \exp\left(\frac{Q}{RT}\right) \tag{2}$$

where R is the molar gas constant (8.3145 J·mol^{-1}·K^{-1}), T is the absolute temperature in Kelvin, Q is the hot deformation activation energy (kJ·mol^{-1}), σ is the flow stress (MPa), $\dot{\varepsilon}$ is the strain rate, Z is a Zener–Hollomon parameter, A, α and n are the material constants, which are independent of the hot deformation temperature.

According to the true stress–true strain curves (Fig. 3), the alloy constants of the constitutive equations were accurately determined. In the study, the strain is 0.5. Regarding the low stress ($\alpha\sigma < 0.8$) and the high stress ($\alpha\sigma > 1.2$) levels, the relationships between the flow stress and the strain rate can be expressed through the following equations [24], respectively:

$$\dot{\varepsilon} = A_1\sigma^{n_1} \exp\left(-\frac{Q}{RT}\right) \quad \text{(low flow stress)} \tag{3}$$

$$\dot{\varepsilon} = A_2 \exp(\beta\sigma) \exp\left(-\frac{Q}{RT}\right) \quad \text{(high flow stress)} \tag{4}$$

where A_1, A_2, n_1 and β are the alloy constants. The relationship among α, β and n_1 can be expressed in Eq. (5).

$$\alpha = \beta/n_1 \tag{5}$$

The parameters in Eq. (1) could be acquired from Eqs. (3)–(5). With the logarithmic consideration of Eqs. (3), (4), Eqs. (6), (7) could be obtained, as presented in Fig. 4. Also, the mean values of n_1 (4.7614) and β value (0.0537) could be calculated from the slopes of the parallel and straight lines in $\ln\sigma$ versus $\ln\dot{\varepsilon}$ and σ versus $\ln\dot{\varepsilon}$ plots.

$$\ln\sigma = \frac{\ln\dot{\varepsilon}}{n_1} - \frac{\ln A_1}{n_1} \tag{6}$$

$$\sigma = \frac{\ln\dot{\varepsilon}}{\beta} - \frac{\ln A_2}{\beta} \tag{7}$$

The value of α (0.0113) could be obtained through Eq. (5). When the deformation temperature (T) is a constant, the logarithms of both sides of Eq. (1) were considered:

$$\ln\dot{\varepsilon} = \ln A + n \ln[\sinh(\alpha\sigma)] - \frac{Q}{RT} \tag{8}$$

Therefore, the Q could be calculated by the following equation:

$$Q = R\left[\frac{\partial \ln\dot{\varepsilon}}{\partial \ln[\sinh(\alpha\sigma)]}\right]_T \left[\frac{\partial \ln[\sinh(\alpha\sigma)]}{\partial(1/T)}\right]_\varepsilon \tag{9}$$

Therefore, the value of Q was determined from the curves of $\ln[\sinh(\alpha\sigma)] - 1000/T$ (Fig. 5b). The $\ln A$ was also easily discovered from the interception of $\ln[\sinh\alpha\sigma] - \ln\dot{\varepsilon}$. The value of n (3.44) could be acquired. The values of Q (245,481.3 J·mol^{-1}) and A (6.58 × 10^{10}) could be calculated through Eqs. (8), (9), and the two values are lower than those in Ref. [6] (Q is 261,719.8 J·mol^{-1} and A is 6.1 × 10^{12}, respectively). The results demonstrate that the larger deformation needs more hot deformation activation energy for the alloy. Subsequently, the $Z = \dot{\varepsilon}\exp(245481.3/RT)$ could be obtained. Finally, the various Z values could be calculated at both various strain rates and deformation temperatures through Eq. (2). Through the linear fitting method, the $\ln Z$ versus $\ln[\sinh(\alpha\sigma)]$ was plotted, as shown in Fig. 6. The plot demonstrates good linear correlations between flow stress and Z value, where $\ln Z = 3.303\ln[\sinh(\alpha\sigma_p)] + 22.2136$. The regression coefficient is 0.989, which indicates the established constitutive equations validity of the Ti–3.0Al–3.5Cr–2.0Fe–0.1B alloys. Based on the aforementioned calculated
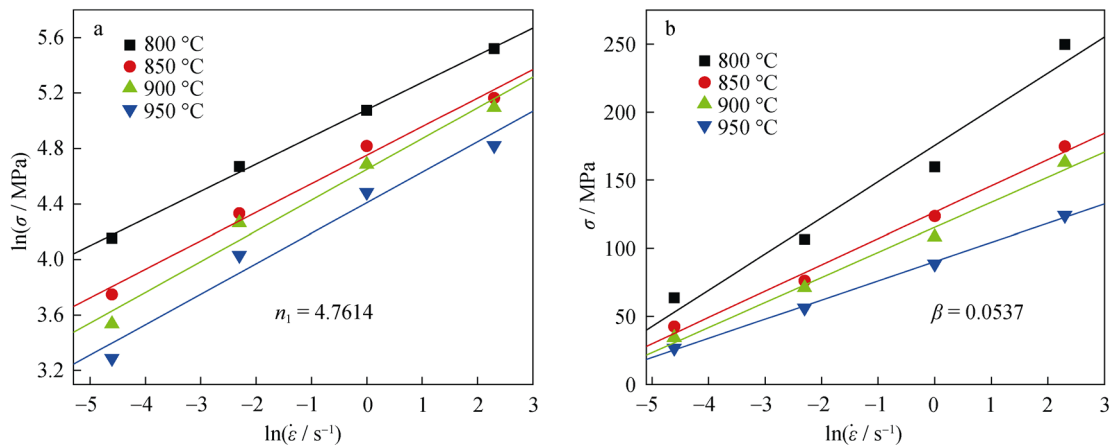
Fig. 4 Relationships between strain rate and peak stress: **a** $\ln\sigma - \ln\dot{\varepsilon}$ and **b** $\sigma - \ln\dot{\varepsilon}$
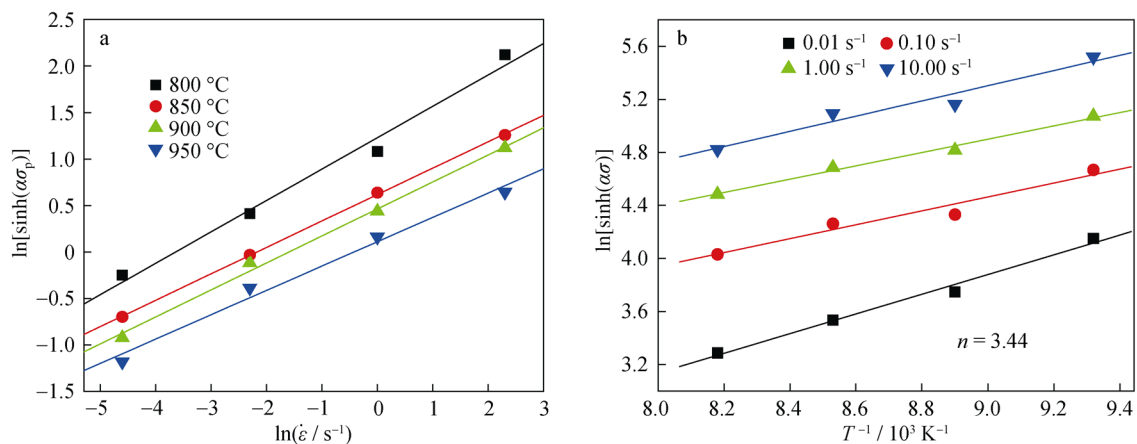

Fig. 5 Relationship between peak stress and deformation temperature: **a** $\ln[\sinh(\alpha\sigma)] - \ln\dot{\varepsilon}$ and **b** $\ln[\sinh(\alpha\sigma)] - 1000/T$
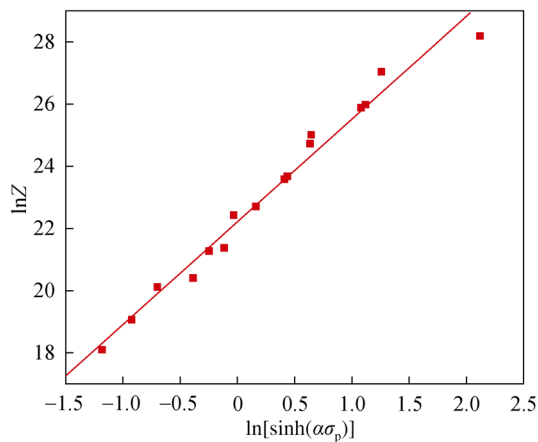

Fig. 6 Relationship between flow stress and Z parameter

parameters, the constitutive equation of the Ti–3.0Al–3.5Cr–2.0Fe–0.1B alloy could be written as:

$$\dot{\varepsilon} = 6.58 \times 10^{10} [\sinh(0.0113\sigma)]^{3.44} \exp(-245481.3/RT).$$

3.3 Processing map

The processing map was developed for the hot deformation process optimization on the basis of the deformation mechanism description and analysis during processing [25]. Figure 7 presents the Ti–3.0Al–3.5Cr–2.0Fe–0.1B alloy processing map at the true strain of 0.693. The processing map includes a superimposition of a power dissipation map and an instability map, which illustrate both "safe" and "unsafe" districts. In Fig. 7, the numbers represent the efficiency percentage of power dissipation and the shaded regions represent the instability domains. It could be observed that the Ti–3.0Al–3.5Cr–2.0Fe–0.1B alloys have a wide processing window. An inflexion of the efficiency contours at approximately 880 °C is observed. This could be attributed to the deformation mechanism change [26, 27]. Beyond 880 °C, the alloy deformation is dominated by the β phase. Below 880 °C, the deformation
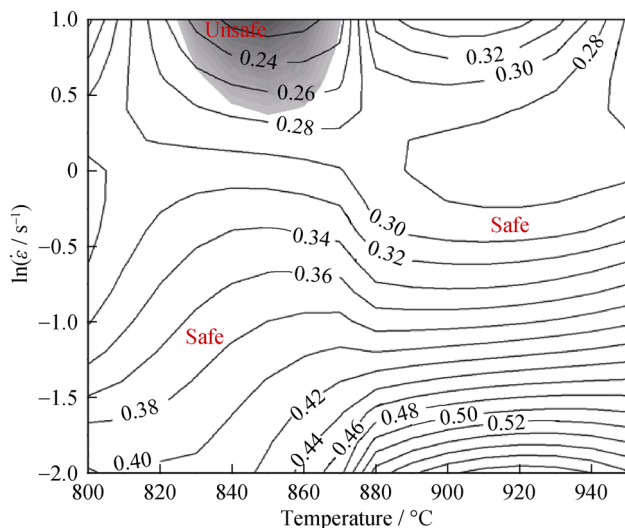
Fig. 7 Processing map of Ti–3.0Al–3.5Cr–2.0Fe–0.1B alloy at true strain of 0.693

is dominated by a coordination between α and β phases. Furthermore, the power dissipation efficiency increases as the temperature increases and the strain rate decreases, which indicates that the deformation requires a higher amount of the absorbed energy at a lower strain rate and a higher temperature [27]. The map demonstrates that the "unsafe" region is at the strain rate of 10.00 s^{-1} and at approximately 850 °C. According to the processing map, the instability region should be avoided during processing. When the compression of the alloy is 70% [6], there is no "unsafe" region in the processing map. The results indicate that a smaller deformation would not necessarily obtain a better result for comparing with a larger deformation.

3.4 Microstructural evolution

The microstructures of Ti–3.0Al–3.5Cr–2.0Fe–0.1B alloys at 850 °C under various strain rates are presented in Fig. 8. It could be observed that the strain rates exhibit remarkable effects on the microstructural evolution under compression. Apparently, the grains are elongated along the vertical direction of the compression direction. At the lower strain rate of 0.01 s^{-1}, the dominant deformation mechanism is dynamic recovery due to the elongated grains existence (Fig. 8a). As the strain rate increases from 0.01 to 0.10 s^{-1}, the grain boundaries become serrated and bulged, whereas a slight dynamic recrystallization occurs in the grain interior and the boundaries (Fig. 8b). Furthermore, the sub-boundaries and subgrains are observed in the grain interior. At the higher strain rate of 1.00 s^{-1}, the dynamic recrystallization of the grains is not apparent, whereas the amounts of both subboundaries and subgrains decrease. As it is known, the dynamic recrystallization is prone to occurring as a result of the dislocation glide/climb process,
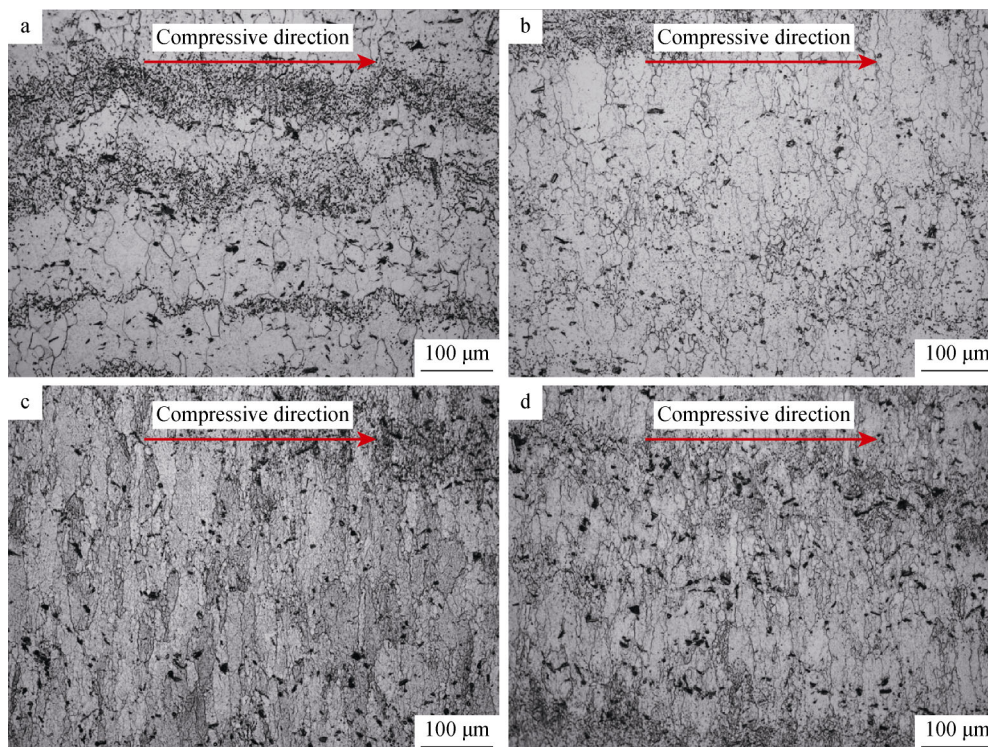

Fig. 8 OM images of deformation microstructure of Ti–3.0Al–3.5Cr–2.0Fe–0.1B alloy at 850 °C under different strain rates: **a** 0.01 s^{-1}, **b** 0.10 s^{-1}, **c** 1.00 s^{-1}, and **d** 10.00 s^{-1}

causing the occurrence of elongated and thin recrystallized grains [28].

It was reported that the accumulated energy increased at high strain rates and there is not enough time to conduct dislocation cross [18]. Therefore, at higher strain rates, the recrystallized grain growth is not remarkable due to the short deformation duration. At lower strain rates, the recrystallized grains have an adequate time frame to nucleate and grow [29, 30]. Hence, the results illustrate that the microstructure of Ti–3.0Al–3.5Cr–2.0Fe–0.1B alloy is significantly dependent on the strain rate.

4 Conclusion

The Ti–3.0Al–3.5Cr–2.0Fe–0.1B beta alloy is sensitive to the strain rate and the deformation temperature. The flow stress rapidly reached the peak stress due to work hardening, at the beginning of the flow stress–strain curves. The peak flow stresses increased as the strain rate increased and decreased as the deformation temperature increased. The constitutive equation of the Ti–3.0Al–3.5Cr–2.0 Fe–0.1B beta alloy was established $\dot{\varepsilon} = 6.58 \times 10^{10} [\sinh (0.0113\sigma)]^{3.44} \exp(-245481.3/RT)$ under the test conditions in this study. At the true strain of 0.693, the Ti–3.0Al–3.5Cr–2.0Fe–0.1B alloy processing map displayed the "unsafe" region at the strain rate of 10 s^{-1} and the deformation temperature at approximately 850 °C, whereas the rest region was "safe." Through the Ti–3.0Al–3.5Cr–2.0Fe–0.1B alloy microstructure observations at the deformation temperature of 850 °C under various strain rates, the dominant deformation mechanism was the dynamic recovery at a lower strain rate, whereas the dynamic recrystallization was the main deformation mechanism at a high strain rate.

References

[1] Song XY, Li Y, Zhang F. Microstructure and mechanical properties of Nb-and Mo-modified NiTi-Al-based intermetallics processed by isothermal forging. Mater Sci Eng A. 2014;594:229.

[2] Wang ZG, Cai HJ, Hui SX. Microstructure and mechanical properties of a novel Ti–Al–Cr–Fe titanium alloy after solution treatment. J Alloys Compd. 2015;640:253.

[3] An Z, Li JS, Feng Y. Optimization of thermal processing parameters of Ti555211 alloy using processing maps based on Murty criterion. Rare Met. 2016;35(2):154.

[4] Sun ZC, Yang H, Han GJ, Fan XG. A numerical model based on internal-state-variable method for the microstructure evolution

during hot-working process of TA15 titanium alloy. Mater Sci Eng A. 2010;527:3464.

[5] Lei LM, Huang X, Wang MM, Wang LQ, Qin JN, Li HP, Lu SQ. Effect of hot compressive deformation on the martensite transformation of Ti–10V–2Fe–3Al titanium alloy. Mater Sci Eng A. 2011;530(1):591.

[6] Wang G, Hui SX, Ye WJ, Mi XJ. Hot compressive behavior of Ti–3.0Al–3.7Cr–2.0Fe–0.1B titanium alloy. Trans Nonferrous Met Soc China. 2012;22(12):2965.

[7] Hua K, Xue XY, Kou HC, Fan JK, Tang B, Li JS. Characterization of hot deformation microstructure of a near beta titanium alloy Ti-5553. J Alloys Compd. 2014;615:531–7.

[8] An Z, Li JS, Feng Y. Microstructure evolution of a new near-b titanium alloy: Ti555211 during high-temperature deformation. Rare Met. 2015;34(11):757.

[9] Tao ZJ, Yang H, Li H, Ma J, Gao PF. Constitutive modeling of compression behavior of TC4 tube based on modified Arrhenius and artificial neural network models. Rare Met. 2016;35(2):162.

[10] Zhao AM, Yang H, Fan XG, Gao PF, Zuo R, Meng M. The flow behavior and microstructure evolution during (α + β) deformation of β wrought TA15 titanium alloy. Mater Design. 2016;109:112.

[11] Gao J, Li MQ, Liu GJ, Liu SF. Deformation behavior and processing maps during isothermal compression of TC21 alloy. Rare Met. 2017;36(2):86.

[12] Wang G, Hui SX, Ye WJ, Mi XJ, Wang YL, Zhang WJ. Microstructure and tensile properties of low cost titanium alloys at different cooling rate. Rare Met. 2012;31(6):531.

[13] Wang G, Hui SX, Ye WJ, Mi XJ. Influence of solution treatment on microstructure and mechanical properties of Ti–3.0Al–2.3Cr–1.3Fe titanium alloy. Chin J Nonferrous Met. 2012;22(8):3015.

[14] Wang G, Hui SX, Ye WJ, Mi XJ. Hot compressive behavior of Ti–3.0Al–3.7Cr–2.0Fe low cost titanium alloy. Chin J Nonferrous Met. 2012;22(8):2223.

[15] Zhang JL, Guo HZ, Liang HQ. Hot deformation behavior and process parameter optimization of Ti22Al25Nb using processing map. Rare Met. 2016;35(1):118.

[16] Qin C, Yao ZK, Ning YQ, Shi ZF, Guo HZ. Hot deformation behavior of TC11/Ti–22Al–25Nb dual-alloy in isothermal compression. Trans Nonferrous Met Soc China. 2015;25(7):2195.

[17] Xu HB, Meng LJ, Xu J, Li Y, Zhao XQ. Mechanical properties and oxidation characteristics of TiNiAl(Nb) intermetallics. Intermetallics. 2007;15(5–6):778.

[18] Lu SQ, Ouyang DL, Cui X, Wang KL. Dynamic recrystallization behavior of burn resistant titanium alloy Ti–25V–15Cr–0.2Si. Trans Nonferrous Met Soc China. 2016;26(4):1003.

[19] Liu B, Liu YG, Qiu CZ, Zhou CX, Li JB, Li HZ, He YH. Design of low-cost titanium aluminide intermetallics. J Alloys Compd. 2015;640:298.

[20] Yu H, Liu SS, Liu LG, Ren WB, Li J. Hot mechanical behavior and deformability of TA17 titanium alloy. Chin J Rare Met. 2017;41(1):2.

[21] Abbasi SM, Momeni A, Lin YC, Jafarian HR. Dynamic softening mechanism in Ti–13V–11Cr–3Al beta Ti alloy during hot compressive deformation. Mater Sci Eng A. 2016;665:154.

[22] Li XF, Huang X, Huang LJ, Sha AX. Deformation behavior of hot compression for TC27 titanium alloy. Rare Met Mater Eng. 2016;45(3):793.

[23] Bobbili R, Ramudu BV, Madhu V. A physically-based constitutive model for hot deformation of Ti-10-2-3 alloy. J Alloys Compd. 2017;696:295.

[24] Pilehva F, Zarei-Hanzaki A, Ghambari M, Abedi HR. Flow behavior modeling of a Ti–6Al–7Nb biomedical alloy during

manufacturing at elevated temperatures. Mater Des. 2013;51(5): 457.

[25] Ma X, Zeng WD, Xu B, Sun Y, Xue C, Han YF. Characterization of the hot deformation behavior of a Ti–22Al–25Nb alloy using processing maps based on the Murty criterion. Intermetallics. 2012;20(1):1.

[26] Wang B, Huang LJ, Geng L, Rong XD. Compressive behaviors and mechanisms of TiB whiskers reinforced high temperature Ti60 alloy matrix composites. Mater Sci Eng A. 2015;648:443.

[27] Li JB, Liu Y, Liu B, Wang Y, Zhao K, He YH. Effect of Nb particles on the flow behavior of TiAl alloy. Intermetallics. 2014;44:22.

[28] Bai XF, Zhao YQ, Zeng WD, Jia ZQ, Zhang YS. Characterization of hot deformation behavior of a biomedical titanium alloy TLM. Mater Sci Eng A. 2014;598:236.

[29] Jiang SY, Zhang YQ, Zhao YN. Dynamic recovery and dynamic recrystallization of NiTi shape memory alloy under hot compression deformation. Trans Nonferrous Met Soc China. 2013; 23(1):140.

[30] Liu N, Li Z, Xu WY, Wang Y, Zhang GQ, Yuan H. Hot deformation behavior and microstructural evolution of powder metallurgical TiAl alloy. Rare Met. 2017;36(2):86.